Structure of the dissipation region in fluid simulations of asymmetric magnetic reconnection[a)]

P. A. Cassak[1,b)] and M. A. Shay[2]
[1]*Department of Physics, West Virginia University, Morgantown, West Virginia 26506, USA*
[2]*Department of Physics and Astronomy, University of Delaware, Newark, Delaware 19716, USA*

(Received 7 December 2008; accepted 2 February 2009; published online 24 March 2009)

The structure of the dissipation region during asymmetric magnetic reconnection is studied assuming antiparallel magnetic fields in two dimensions. A physics-based prediction for the scaling of the thickness of the dissipation region in (collisionless) Hall reconnection is presented and confirmed with two-fluid simulations. However, the substructure of the dissipation region in these and additional single-fluid (magnetohydrodynamics) simulations disagrees with a recent model [Cassak and Shay, Phys. Plasmas **14**, 102114 (2007)]. We attribute the disagreement to the lack of plasma mixing along newly reconnected field lines in fluid models, rendering the use of a fluid description of questionable validity for determining the dissipation region substructure. Applications to the dayside magnetopause are discussed. © *2009 American Institute of Physics*.
[DOI: 10.1063/1.3086867]

I. INTRODUCTION

Early work on magnetic reconnection[1–4] assumed a high degree of symmetry to make the problem tractable. However, the generic configuration for reconnection involves asymmetries, including differing densities and magnetic field strengths on the two sides of the dissipation region where the frozen-in condition breaks down. The most glaring example is at the dayside magnetopause.[5–9] Plasmaspheric drainage plumes[10] can affect reconnection at the dayside[11] and asymmetries also impact flux transfer events.[12] Other examples include the distant magnetotail,[13] the solar wind,[14] tokamaks,[15,16] the solar corona,[17] and turbulence.[18]

The first studies of asymmetries addressed the shock structure of fast reconnection at the dayside magnetopause,[5] initiating vigorous research both in theoretical and numerical studies (see Ref. 19 for references). More recent studies considered the effect of asymmetries on the out-of-plane magnetic field profile[20] and the impact of diamagnetic drifts on reconnection.[21]

Recently, studies have considered the scaling (meaning the functional dependence on system parameters) of the properties of asymmetric reconnection. Borovsky and Hesse[22] studied the reconnection rate as a function of density asymmetry. Cassak and Shay[19] performed a Sweet–Parker-type analysis predicting the scaling of the reconnection rate E, outflow speed v_{out}, and the structure of the dissipation region (defined as the shape of the dissipation region and the location of the X-line and stagnation point). The analysis considered reconnection only between antiparallel fields in two dimensions.

The predictions have been tested for asymmetric density,[22] asymmetric fields,[19] both asymmetric,[23] and in a global magnetospheric geometry[24] with resistive magnetohydrodynamic (MHD) simulations, for all combinations of asymmetries in two-fluid (Hall-MHD with electron inertia) simulations of (collisionless) Hall reconnection,[25] and with particle-in-cell (PIC) simulations.[26] The prediction for E and v_{out} has performed very well, as has the prediction that the X-line and stagnation point are decoupled.[19,23,25,26]

Recently, other fundamental physics studies of asymmetric reconnection were performed with PIC simulations,[26–29] observations at the dayside magnetopause,[30] and comparisons between the two.[27,31] In addition, the scaling result for E was used[32] to develop a quantitative prediction of solar wind-magnetospheric coupling. Despite the use of a simplistic model to extrapolate the two-dimensional theory to three dimensions, the correlation between solar wind data and geomagnetic indices was as good as the best previous model, one which used unphysical fitting techniques to achieve its agreement. This suggests that a quantitative understanding of asymmetric reconnection can be of great importance for magnetospheric applications.

The theory has enjoyed less success in its prediction of the substructure of the dissipation region. In particular, the theory predicts that the stagnation point can be on either side of the X-line depending on the parameters, but Ref. 23 found that the stagnation point was always on the low field side. Also, the scaling of the thickness of the dissipation region during Hall reconnection is unknown.

This paper addresses the structure of the dissipation region during asymmetric reconnection. We present a physical model for the dissipation region thickness during Hall reconnection. The model is compared to two-fluid simulations, finding good agreement. However, the location of the stagnation point in the simulations (as well as in new resistive MHD simulations with asymmetric density) is inconsistent with the theory from Ref. 19, similar to the results in Ref. 23. We argue that the cause of the inconsistency is the failure of fluid models to allow mixing of plasma along newly reconnected field lines. Kinetic simulations, which allow mixing,[33]

[a)]Paper JI1, Bull. Am. Phys. Soc. **53**, 119 (2008).
[b)]Invited speaker.

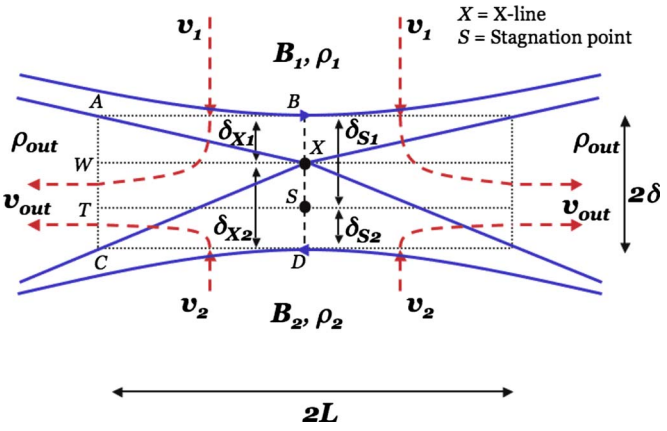

FIG. 1. (Color online) Schematic of the dissipation region during asymmetric reconnection. Magnetic field lines are (blue) solid lines; velocity flow are (red) dashed lines. The points X and S mark the X-line and the stagnation point, which are not necessarily colocated. Reprinted from Ref. 19.

are needed to resolve the theory of the dissipation region substructure.

The theory from Ref. 19 is reviewed in Sec. II, followed by a model for the structure of the dissipation region in Hall reconnection. Results of two-fluid simulations of Hall reconnection and MHD simulations of Sweet–Parker reconnection (with uniform resistivity) with asymmetric density are presented in Sec. III. Limitations of fluid models are discussed in Sec. IV. Section V contains applications and conclusions.

II. THEORY

It was recently shown that the scaling of the outflow speed v_{out} and reconnection rate E during asymmetric reconnection follows directly from conservation of mass, energy, and magnetic flux into and out of the dissipation region,[19]

$$v_{out}^2 \sim \frac{B_1 B_2}{4\pi}\frac{B_1+B_2}{\rho_1 B_2+\rho_2 B_1}, \tag{1}$$

$$E \sim \left(\frac{B_1 B_2}{B_1+B_2}\right)\frac{v_{out}}{c}\frac{2\delta}{L}, \tag{2}$$

where the (half-) thickness and length of the dissipation region are δ and L, the upstream magnetic field strength is B, and the mass density is ρ. The "1," "2," and "out" subscripts refer to properties upstream and above, upstream and below, and in the outflow region, respectively, and "$\sim$" means "scales like." In writing Eq. (2), we have taken the outflow density ρ_{out} to scale as[19]

$$\rho_{out} \sim \frac{\rho_1 B_2+\rho_2 B_1}{B_1+B_2}, \tag{3}$$

which follows from assuming that (1) the plasma is incompressible and (2) the plasmas on either side of the dissipation region mix completely along a newly reconnected field line before exiting the dissipation region. [See Ref. 34 for an alternate derivation of Eq. (1).]

The interior structure of the dissipation region also follows from conservation laws.[19] Define, following Fig. 1, δ_{X1} and δ_{X2} as the distances from the upstream edges of the dissipation region to the X-line and δ_{S1} and δ_{S2} from the edges to the stagnation point. The energy flux through a box from the edge of the dissipation region to the neutral line ($ABXW$ and $CDXW$ in Fig. 1) gives

$$L\left(\frac{B_1^2}{8\pi}v_1\right) \sim \delta_{X1}\left(\frac{1}{2}\rho_{out}v_{out}^2\right)v_{out}, \tag{4}$$

$$L\left(\frac{B_2^2}{8\pi}v_2\right) \sim \delta_{X2}\left(\frac{1}{2}\rho_{out}v_{out}^2\right)v_{out}, \tag{5}$$

which follows because there is no magnetic energy flux across XW. Similarly, the mass flux through boxes from the upstream edges of the dissipation region to the stagnation point ($ABST$ and $CDST$) gives

$$L(\rho_1 v_1) \sim \delta_{S1}(\rho_{out}v_{out}), \tag{6}$$

$$L(\rho_2 v_2) \sim \delta_{S2}(\rho_{out}v_{out}), \tag{7}$$

which follows because there is no mass flux across ST.

Taking the ratio of Eq. (5) to (4) and using $v_1 B_1 \sim v_2 B_2$ from the conservation of flux yields

$$\frac{\delta_{X2}}{\delta_{X1}} \sim \frac{B_2}{B_1}. \tag{8}$$

Similarly, the ratio of Eq. (7) to (6) gives

$$\frac{\delta_{S2}}{\delta_{S1}} \sim \frac{\rho_2 B_1}{\rho_1 B_2}. \tag{9}$$

These two relations give the *relative* interior structure of the dissipation region. The considerations thus far are independent of dissipation mechanism, so should hold for any model of reconnection. To get the absolute structure, a particular model of reconnection must be considered. We treat Sweet–Parker and Hall reconnection in turn.

A. Structure of the dissipation region in asymmetric Sweet–Parker reconnection

During asymmetric Sweet–Parker reconnection, a nonzero resistivity breaks the frozen-in condition. From Faraday's law, $v_1 \sim \eta c^2/4\pi\delta_{X1}$ (and $v_2 \sim \eta c^2/4\pi\delta_{X2}$). Using Eq. (2), Eq. (8), $E \sim v_1 B_1/c$, and $2\delta = \delta_{X1}+\delta_{X2}$, one finds[19]

$$\delta_{X1} \sim \sqrt{\frac{\eta c^2 L}{4\pi v_{out}}\frac{B_1}{B_2}} \quad \text{and} \quad \delta_{X2} \sim \sqrt{\frac{\eta c^2 L}{4\pi v_{out}}\frac{B_2}{B_1}}. \tag{10}$$

The half thickness δ of the layer is, therefore,

$$\delta \sim \frac{1}{2}\left(\sqrt{\frac{B_1}{B_2}}+\sqrt{\frac{B_1}{B_2}}\right)\sqrt{\frac{\eta c^2 L}{4\pi v_{out}}}. \tag{11}$$

For completeness, the reconnection rate is

$$E \sim \frac{1}{c}\sqrt{\frac{\eta c^2 v_{out}}{4\pi L}B_1 B_2}. \tag{12}$$

As noted in Ref. 19, these results generalize the Sweet–Parker scaling results[3] to asymmetric systems.

B. Structure of the dissipation region in asymmetric Hall reconnection

In symmetric anti-parallel Hall reconnection, the thickness of the ion dissipation region scales with the ion inertial length, $\delta \sim d_i = c/\omega_{pi}$, as has been argued on physical grounds[35,36] and confirmed by simulations[37] and laboratory experiments.[38–40] This length scale arises physically because an ion of mass m_i and charge e entering the dissipation region gets accelerated in the out-of-plane direction by the reconnection electric field E and undergoes gyromotion around the newly reconnected magnetic field B_y. To see how this arises, note that the transit time through the dissipation region is $\Delta t \sim L/v_{\rm out}$. Then, the speed in the out-of-plane direction reached due to the free acceleration is $v_z \sim eE\Delta t/m_i$. Using $E \sim v_{\rm in}B_x/c$ from Ohm's law and $\delta \sim L(v_{\rm in}/v_{\rm out})$ from mass continuity gives

$$v_z \sim \frac{e}{m_i}\left(\frac{v_{\rm in}B_x}{c}\right)\frac{L}{v_{\rm out}} \sim \Omega_{\rm ci}(B_x)\delta, \tag{13}$$

where $\Omega_{\rm ci}(B_x) = eB_x/m_ic$ is the ion cyclotron frequency in the reconnecting magnetic field B_x. Since $v_z \sim v_{\rm out}$, which follows from the z component of the momentum equation (or from the particle picture by noting that the particle is merely redirected by B_y to generate the outflow) and $v_{\rm out} \sim c_A$, the Alfvén speed based on the reconnecting field B_x, one finds

$$\delta \sim \frac{c_A}{\Omega_{\rm ci}(B_x)} \sim d_i. \tag{14}$$

We conjecture that similar physics controls the thickness of the dissipation region in asymmetric reconnection. An ion entering the dissipation region is accelerated by the reconnection electric field E given by Eq. (2) to the outflow speed $v_{\rm out}$ in Eq. (1). Using these results in the same expression as before, $v_z \sim eE\Delta t/m_i$, yields

$$v_z \sim \frac{e}{m_ic}\left(\frac{2B_1B_2}{B_1+B_2}\right)\delta \sim \Omega_{\rm ci}(B_{\rm red})\delta, \tag{15}$$

where $B_{\rm red} = 2B_1B_2/(B_1+B_2)$ is the reduced magnetic field. Using $v_z \sim v_{\rm out}$, we obtain

$$\delta \sim \frac{v_{\rm out}}{\Omega_{\rm ci}(B_{\rm red})}. \tag{16}$$

From Eq. (1), this can be written as

$$\delta \sim \frac{1}{2}\left(\sqrt{\frac{B_1}{B_2}} + \sqrt{\frac{B_2}{B_1}}\right)d_{i,\rm out} \sim \left(\frac{B_{\rm geo}}{B_{\rm red}}\right)d_{i,\rm out}, \tag{17}$$

where $d_{i,\rm out} = (m_i^2c^2/4\pi e^2\rho_{\rm out})^{1/2}$ is the ion inertial length based on the outflow density given in Eq. (3) and $B_{\rm geo} = (B_1B_2)^{1/2}$ is the geometric mean of the magnetic fields. The magnetic prefactor is the same as in Eq. (11) and is always larger than 1, so δ is always greater than or equal to $d_{i,\rm out}$; physically, this is because an increase in one of the magnetic fields increases the outflow speed, which increases the gyroradius. We expect an expression similar to Eq. (17) to hold for the electron layer, but this will not be pursued in the present study. The relative location of the X-line and stagnation point (for both ions and electrons in their respective dissipation regions) should obey Eqs. (8) and (9) because their derivation is independent of dissipation mechanism.

III. NUMERICAL SIMULATIONS AND RESULTS

A. Code and simulations

We use the massively parallel code F3D (Ref. 41) to perform two-dimensional simulations of asymmetric Sweet–Parker and Hall reconnection. The density, ion velocity, magnetic field, and ion pressure are evolved explicitly using the trapezoidal leapfrog in time and fourth order finite difference in space. Magnetic field strengths, mass densities, velocities, electric fields, and pressures are normalized to B_0, ρ_0, the Alfvén speed $c_{A0} = B_0/(4\pi\rho_0)^{1/2}$, $E_0 = c_{A0}B_0/c$, and $P_0 = \rho_0 c_{A0}^2$, respectively. In the MHD runs, lengths are normalized to an arbitrary length L_0; resistivities are normalized to $\eta_0 = 4\pi c_{A0}L_0/c^2$. In the two-fluid runs, lengths are normalized to the ion inertial length $d_{i0} = (m_i^2c^2/4\pi\rho_0e^2)^{1/2}$.

The computational domain for both sets of simulations has a size $L_x \times L_y = 204.8 \times 102.4$ with a cell size of 0.05×0.05 (in the appropriate units) and uses periodic boundary conditions. The initial magnetic field profile is an asymmetric double tearing mode configuration,

$$B_x(y) = \begin{cases} -B_{01}\tanh\left(\dfrac{y - L_y/4}{w_0}\right), & \dfrac{L_y}{4} < y < \dfrac{L_y}{2} \\ -B_{02}\tanh\left(\dfrac{y - L_y/4}{w_0}\right), & 0 < y < \dfrac{L_y}{4}, \end{cases} \tag{18}$$

where B_{01} and B_{02} are initial asymptotic magnetic fields and $w_0 = 2.0$ is the initial current sheet thickness. There is no initial out-of-plane (guide) magnetic field. The initial density profile is

$$\rho(y) = \frac{\rho_{01}+\rho_{02}}{2} + \frac{\rho_{01}-\rho_{02}}{2}\tanh\left(\frac{y - L_y/4}{w_0}\right) \tag{19}$$

for $0 < y < L_y/2$, with asymptotic values ρ_{01} and ρ_{02}. The initial pressure P enforces global pressure balance, $P(y) + [B_x(y)]^2/8\pi = \text{constant}$. The constant is $P_{\rm min} + B_{\rm max}^2/8\pi = (B_{\rm max}^2/8\pi)(1+\beta_{\rm min})$, where $B_{\rm max} = \max(B_{01}, B_{02})$, $P_{\rm min}$ is the minimum pressure, and $\beta_{\rm min} = P_{\rm min}/(B_{\rm max}^2/8\pi)$ is the minimum plasma beta. The choice of $\beta_{\rm min}$, therefore, specifies the initial profile. The initial temperature $T = P/\rho$ is asymmetric as needed. The double tearing mode is set up by reflecting the profiles about $y=0$ to obtain B_x, ρ, and P for $-L_y/2 < y < 0$. We use $\beta_{\rm min} = 4$, chosen for numerical purposes. We do not expect the results to change for smaller values, but it should be checked in future work.

Reconnection is initiated using a field perturbation of $\delta\mathbf{B} = -(0.01B_0L_y/2\pi)\hat{\mathbf{z}} \times \nabla[\sin(2\pi x/L_x)\sin^2(2\pi y/L_y)]$. The ratio of specific heats γ is 5/3. There is no viscosity, but fourth order diffusion with coefficient 6.25×10^{-6} is used in all of the equations to damp noise at the grid scale. Initial random perturbations on the magnetic field of amplitude 0.000 05 B_0 and on the velocity of amplitude 0.08 c_{A0} break the symmetry so that secondary magnetic islands are ejected.

TABLE I. Asymmetric Hall (*H*) and Sweet–Parker (*SP*) reconnection simulations performed.

Label	B_{01}	B_{02}	ρ_{01}	ρ_{02}	P_{01}	P_{02}	T_{01}	T_{02}	β_{01}	β_{02}
*H*Sym	1	1	1	1	2	2	2	2	4	4
*HB*1	1	2	1	1	9.5	8	9.5	8	19	4
*HB*2	1	3	1	1	22	18	22	18	44	4
*HB*3	0.5	1	1	1	2.375	2	2.375	2	19	4
*HN*1	1	1	1	2	2	2	2	1	4	4
*HN*2	1	1	1	3	2	2	2	0.667	4	4
*HN*3	1	1	0.5	1	2	2	2	4	4	4
*HBN*1	1	2	2	1	8	2	8	4.75	4	19
*SP*Sym	1	1	1	1	2	2	2	2	4	4
*SPN*1	1	1	1	2	2	2	2	1	4	4
*SPN*2	1	1	1	3	2	2	2	0.667	4	4
*SPN*3	1	1	1	4	2	2	2	0.5	4	4
*SPN*4	1	1	1	5	2	2	2	0.4	4	4
*SPN*5	1	1	2	4	2	2	1	0.5	4	4

The two-fluid simulations use an electron inertia of $m_e = m_i/25$, while the MHD simulations employ a constant and uniform resistivity $\eta = 0.015\,\eta_0$.

The standard two-fluid implementation[41] includes electron inertia by assuming negligible ion velocity and uniform density over the small length scales at which the inertia term is appreciable. We adopt the same convention with a fixed density of ρ_0. As such, the simulations do not capture electron scale physics, so the analysis is restricted to ions. Improving on this would require extending the two-fluid formalism to capture density gradients at electron scales or utilizing PIC simulations.

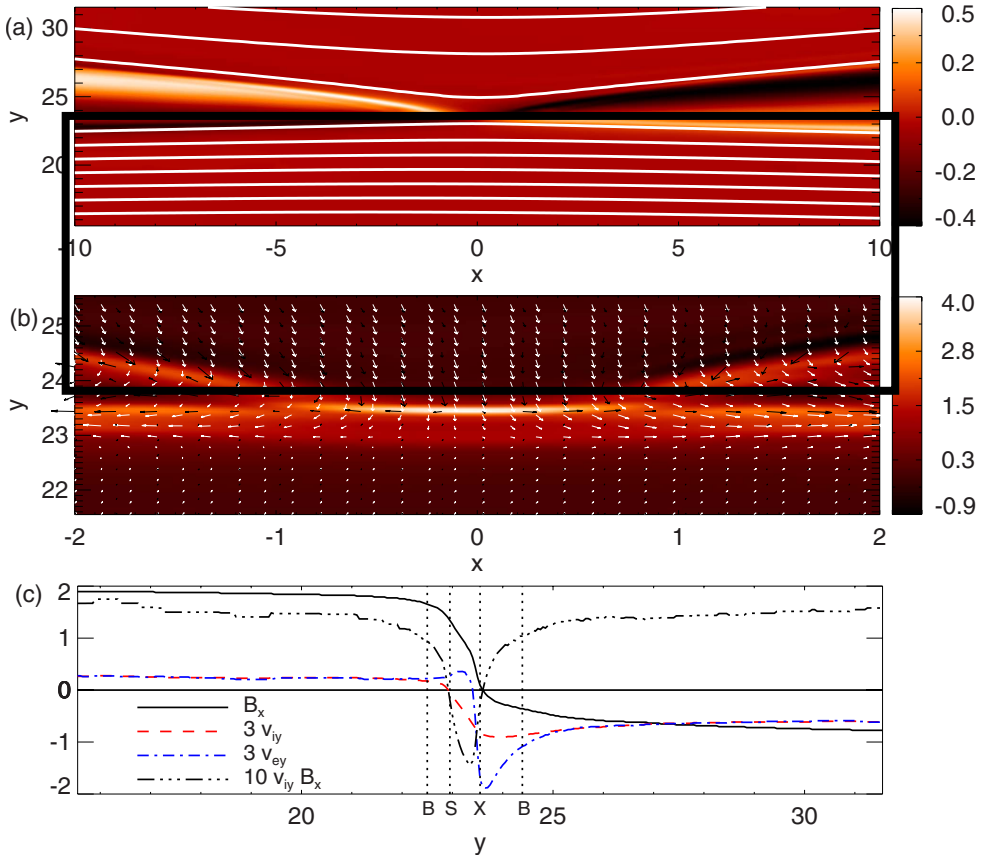

FIG. 2. (Color online) Two-fluid simulation with a magnetic field asymmetry of 2 and symmetric density (run *HB*1). (a) Out-of-plane magnetic field B_z (grayscale) and magnetic field lines (white lines). (b) Out-of-plane current density J_z (grayscale), with ion flow (white arrows) and electron flow (black arrows). Note that the two plots show different domains. (c) A cut across the *X*-line showing the reconnecting magnetic field B_x (solid black line), three times the ion (red dashed) and electron (blue dot-dashed) inflow speeds in the reference frame of the *X*-line, and ten times the convection electric field $v_{iy}B_x$ (dot-dot-dot-dashed).

TABLE II. Measured quantities during asymmetric Hall reconnection simulations. See the text for normalization.

H label $B_{01}(\rho_{01})$, $B_{02}(\rho_{02})$	Sym 1(1),1(1)	$B1$ 1(1),2(1)	$B2$ 1(1),3(1)	$B3$ 0.5(1),1(1)	$N1$ 1(1),1(2)	$N2$ 1(1),1(3)	$N3$ 1(0.5),1(1)	$BN1$ 1(2),2(1)
B_1	0.72	0.37	0.24	0.20	0.72	0.63	0.74	0.37
B_2	0.73	1.60	2.51	0.81	0.72	0.65	0.74	1.56
ρ_1	0.99	0.99	0.99	0.98	0.99	0.98	0.49	1.93
ρ_2	0.98	0.99	1.00	0.99	1.97	2.94	0.98	0.99
E	0.059	0.129	0.171	0.027	0.045	0.037	0.069	0.086
$v_{i,\mathrm{out}}$	0.69	1.03	1.25	0.54	0.52	0.47	0.73	0.79
$v_{e,\mathrm{out}}$	2.07	2.74	3.22	1.32	1.60	1.41	2.93	1.92
v_{yX}	0.000	0.014	0.018	0.010	0.002	0.004	0.000	0.007
δ	0.45	0.56	0.75	0.55	0.37	0.28	0.49	0.42
δ_{X1}	0.43	0.28	0.23	0.29	0.41	0.30	0.55	0.21
δ_{X2}	0.47	0.84	1.27	0.82	0.32	0.26	0.43	0.63
δ_{S1}	0.44	0.97	1.37	0.95	0.41	0.30	0.55	0.74
δ_{S2}	0.45	0.15	0.13	0.15	0.32	0.26	0.43	0.10
L	4.27	5.14	6.11	5.30	4.25	5.40	5.42	3.68

A summary of the simulations performed is in Table I for both Hall (H) and Sweet–Parker reconnection runs. For both sets, Sym denotes a reference symmetric simulation, N denotes asymmetric density, B denotes asymmetric field, and BN denotes both asymmetric. A second HBN simulation included in the scaling study of Ref. 25 is omitted from the present analysis because the density asymmetry is too large to be reliable for the present grid scale (see Ref. 25 for a discussion). For all simulations, the system is evolved until transient effects have subsided and a quasisteady state is achieved. Data are averaged over an extended steady time.

B. Asymmetric Hall reconnection results

The results of the $HB1$ simulation with an asymmetry of two in the magnetic field are shown in Fig. 2. Plot (a) shows the out-of-plane magnetic field B_z with in-plane field lines plotted in white. As has been previously noted,[13,20,21,27,28,30,31,33,42] the quadrupole out-of-plane magnetic field B_z characteristic of Hall reconnection becomes more bipolar when the field is asymmetric. Plot (b) shows the out-of-plane current density J_z with arrows denoting the ion (white) and electron (black) flow pattern. Both the ions and electrons flow through the X-line, implying that the X-line and the stagnation point are not colocated, as predicted in Ref. 19. This is seen more clearly in (c), showing three times the ion (red dashed line) and electron (blue dot dashed) inflow speeds v_{iy} and v_{ey} in a cut across the X-line in the X-line's frame of reference, along with the reconnecting magnetic field B_x (black solid). The X-line is located where B_x goes through zero, marked by the vertical line labeled X. The stagnation point is located where v_{iy} goes through zero (in the moving frame of reference as discussed later), marked by the vertical line labeled "S." The decoupling of the X-line and stagnation point evidenced by a flow through the X-line has been observed in MHD,[19,22,23,25,43–47] hybrid,[33] and PIC simulations,[26] and analytical theory.[15,48] As pointed out in Ref. 25, the ion and electron stagnation points are at different locations.

The raw measured values from the two-fluid simulations are compiled in Table II. The scaling of the reconnection rate E and ion and electron outflow speeds $v_{i,\mathrm{out}}$ and $v_{e,\mathrm{out}}$ were shown to agree with the theory in a previous publication[25] under the assumption that the aspect ratio of the dissipation region δ/L is independent of asymmetries. The length L can be determined from the simulations by finding the location that the convective electric field falls below half the reconnection electric field E in a cut in the outflow direction through the X-line. The values determined in this way are consistent with $\delta/L \sim 0.1$ essentially independent of the field and density asymmetries (although this agreement is extremely sensitive to the method used to define L).

To extract measurements for the structure of the dissipation region, the X-line is found by locating the saddle point in the flux function ψ. The densities ρ_1 and ρ_2 are defined as the average value $2-4\ d_{i0}$ upstream of the X-line, and in all cases are very close to the asymptotic values ρ_{01} and ρ_{02}. One must be careful to measure quantities related to the inflow velocity in the reference frame of the X-line, which moves if the magnetic fields are asymmetric.[17,19,25,44,45,49] To find the speed of the X-line, one measures the magnetic field $B_{1,\mathrm{far}}$ and $B_{2,\mathrm{far}}$ and the ion velocity $v_{1,\mathrm{far}}$ and $v_{2,\mathrm{far}}$ a good distance upstream of the dissipation region. Then, the convective electric fields upstream are $E_1 = v_{1,\mathrm{far}} B_{1,\mathrm{far}}/c$ and $E_2 = v_{2,\mathrm{far}} B_{2,\mathrm{far}}/c$. By assuming that the velocity of the X-line is v_{yX} and that the electric field in the moving frame is uniform and equal to E, one can solve two equations with two unknowns to find

$$v_{yX} = c\frac{E_1 - E_2}{B_{1,\mathrm{far}} + B_{2,\mathrm{far}}}, \tag{20}$$

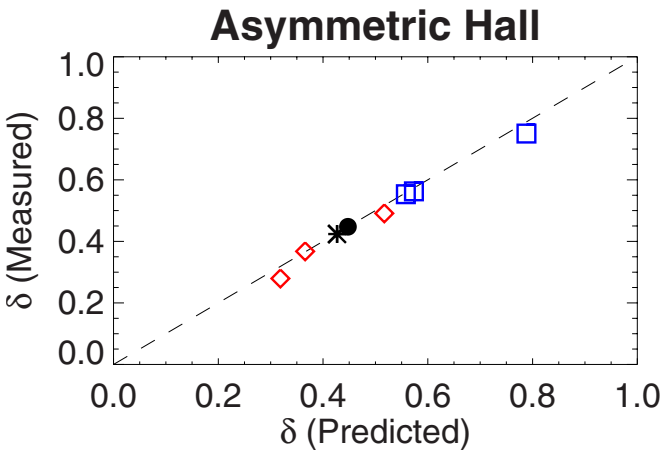

FIG. 3. (Color online) Predicted and measured values for the half-thickness δ of the dissipation region during asymmetric Hall reconnection. The filled circle corresponds to the symmetric reference case *H*Sym; the (blue) squares are runs with asymmetric B (*HB*); the (red) diamonds are runs with asymmetric ρ (*HN*), and the asterisk is the run with both ρ and B asymmetric (*HBN*).

$$E = \frac{E_1 B_{2,\mathrm{far}} + E_2 B_{1,\mathrm{far}}}{B_{1,\mathrm{far}} + B_{2,\mathrm{far}}}. \tag{21}$$

The former was used in an observational study of reconnection at the dayside magnetopause.[8] A consistency check is done by comparing E obtained this way to that obtained from the time rate of change of the flux. The agreement is typically much better than 1%. Also, v_{yX} can be compared to dy_X/dt, where y_X is the y coordinate of the X-line, finding adequate agreement.

The edges of the ion dissipation region are defined as the location, in the moving frame of the X-line, at which $v_{iy}B_x/c$ exceeds half of the reconnection electric field E. Then, δ is defined as half the total distance. The quantities δ_{X1} and δ_{X2} are defined as the distance from either edge to the X-line and δ_{S1} and δ_{S2} are the distances from either edge to the stagnation point.

Finally, the upstream magnetic field strengths B_1 and B_2 used in the scaling analysis are defined as the reconnecting magnetic field B_x a distance $3\delta_{X1}$ upstream of the X-line on the low field side and $3\delta_{S2}$ upstream of the stagnation point on the high field side, marked as the vertical lines labeled "B" in the figure. While the absolute magnitude of the field is sensitive to the particular technique used, the scaling results are not. The magnetic field values obtained this way are significantly smaller than the asymptotic fields, especially for the asymmetric field simulations. This is because, in the simulations, the smaller magnetic field starts to decrease from its asymptotic value far upstream of the dissipation region, an effect compensated by an increase in ion flow (to keep E constant), as is seen in Fig. 2(c). Only at smaller upstream distances do the ion and electron flow decouple, marking the edge of the ion dissipation region. The fields where the ions and electrons decouple are the appropriate fields to use in determining the dissipation region structure. For determining the scaling of E and v_{out} in Ref. 25, the asymptotic fields B_{01} and B_{02} were used.

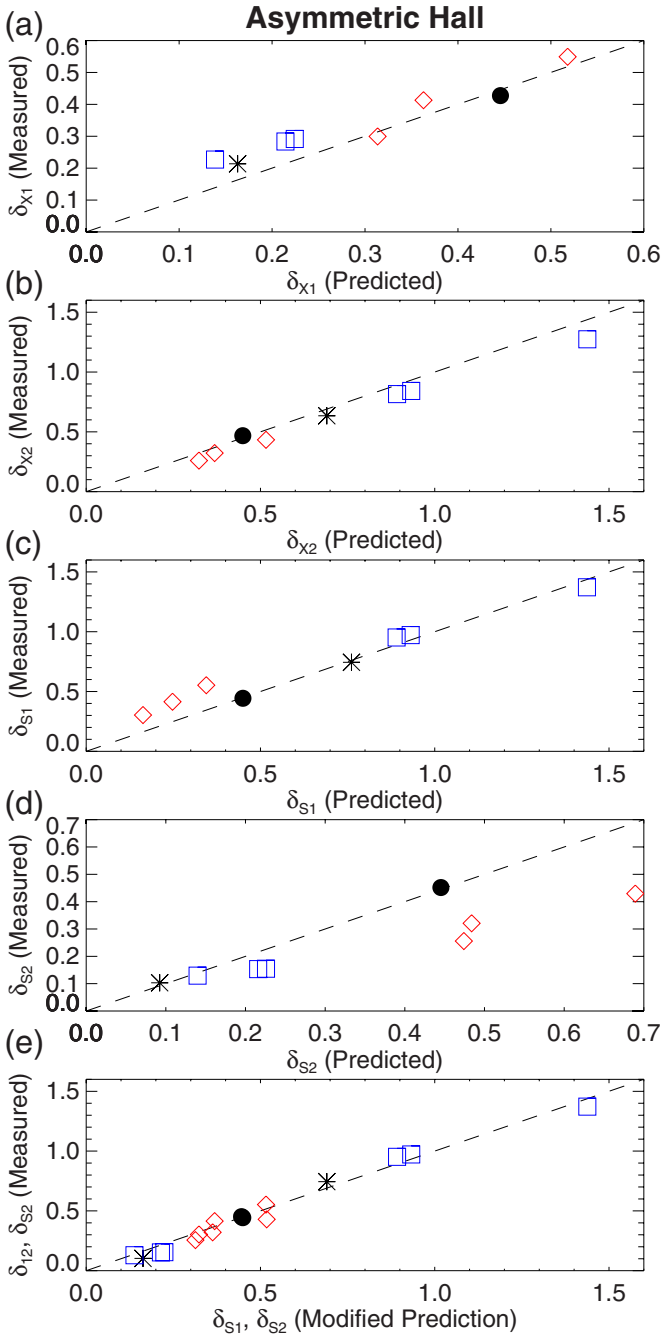

FIG. 4. (Color online) Predictions vs simulation data for the dissipation region substructure: (a) δ_{X1}, (b) δ_{X2}, (c) δ_{S1}, (d) δ_{S2}, and (e) modified prediction for δ_{S1} and δ_{S2}. See Fig. 3 for symbol definitions.

The scaling results for the dissipation region structure are plotted in Figs. 3 and 4. For both plots, the filled circles are for the reference simulation (*H*Sym), the (blue) squares are for asymmetric field (*HB*), the (red) diamonds are for asymmetric density (*HN*), and the asterisk is for both asymmetric (*HBN*). For all plots, the y axis has the length scale in question measured from the simulations and the x axis has the theoretical prediction.

The half-thickness δ of the dissipation region is plotted in Fig. 3. From Eq. (17), the predicted value relative to the reference run is

TABLE III. Measured quantities from the asymmetric density Sweet–Parker simulations. See the text for normalization.

SP label	Sym	*N*1	*N*2	*N*3	*N*4	*N*5
ρ_{01}, ρ_{02}	1,1	1,2	1,3	1,4	1,5	2,4
B_1	0.92	0.89	0.89	0.88	0.87	0.84
B_2	0.93	0.89	0.88	0.87	0.86	0.85
ρ_1	1.00	1.01	1.01	1.01	1.02	2.04
ρ_2	1.00	2.00	3.01	4.02	5.04	4.05
E	0.0134	0.0109	0.0105	0.0103	0.0094	0.0082
v_{out}	0.70	0.53	0.47	0.44	0.42	0.34
v_{yX}	0.000	0.000	0.001	0.001	0.001	0.000
δ	0.86	0.95	1.03	1.08	1.11	1.22
δ_{X1}	0.85	0.94	1.03	1.07	1.09	1.23
δ_{X2}	0.87	0.96	1.03	1.09	1.13	1.22
δ_{S1}	0.85	0.94	1.03	1.08	1.10	1.23
δ_{S2}	0.87	0.96	1.03	1.08	1.13	1.22

$$\delta \sim \delta(\text{Sym})\frac{1}{2}\left(\sqrt{\frac{B_1}{B_2}}+\sqrt{\frac{B_2}{B_1}}\right)\left[\frac{\rho(\text{Sym})}{\rho_{\text{out}}}\right]^{1/2}, \tag{22}$$

where ρ_{out} is given by Eq. (3). The agreement for the total thickness of the dissipation region is very good.

The internal structure, quantified by δ_{X1}, δ_{X2}, δ_{S1}, and δ_{S2}, is plotted in Figs. 4(a)–4(d). The dashed lines denote their predicted equality from Eqs. (8) and (9). The asymmetric field (*HB*) simulations are in pretty good agreement for both the location of the *X*-line and stagnation point. There is some scatter in δ_{X1} and δ_{S2}, but these distances are very small and are susceptible to random error in their determination. For the asymmetric density (*HN*) simulations, the location of the *X*-line matches the theory pretty well. However, the location of the stagnation point shows significant departures from the theory. These results corroborate the results of Ref. 23 which found that the theory did not correctly predict the location of the stagnation point when density is asymmetric.

In anticipation of the discussion of the cause of the disagreement to be presented in Sec. IV, the stagnation point data in plots (c) and (d) are combined in a single plot (e) for comparison with a modified prediction of

$$\frac{\delta_{S2}}{\delta_{S1}} \sim \frac{B_1}{B_2}. \tag{23}$$

The asymmetric density results are in very good agreement with the modified theory. We discuss the physical motivation for the modified theory in Sec. IV.

C. Asymmetric Sweet–Parker reconnection results

The measured quantities from asymmetric density resistive MHD simulations are compiled in Table III. While we are mostly interested in the location of the stagnation point, we consider the other scaling predictions for completeness. The reconnection rate E measured as the time rate of change of ψ compares favorably with a directly measured value of ηJ_X, where J_X is the out-of-plane current density evaluated at the *X*-line. From Eq. (12) evaluated with symmetric fields, we can write

$$E\left[\frac{\rho_1}{\rho_1(\text{Sym})}\right]^{1/4} \sim E(\text{Sym})\left(\frac{2}{1+\rho_2/\rho_1}\right)^{1/4} \tag{24}$$

by dividing it by the same equation evaluated for the symmetric (Sym) run (assuming fixed η and L). This predicts that if $E\rho_1^{1/4}$ is plotted against ρ_2/ρ_1, the data will fall on a single curve. The data are plotted in Fig. 5(a), with the predicted curve plotted as the dotted line. The density is measured as the average value $2-4\ L_0$ upstream of the dissipation region, but it is very close to ρ_{01} and ρ_{02}. For all asymmetric density Sweet–Parker plots to be shown, the filled circles are runs with $\rho_{01}=\rho_0$, while the unfilled square has $\rho_{01}=2\rho_0$. The simulation results are consistent with the theory, in agreement with previous simulations of asymmetric density reconnection in MHD with an artificial localized resistivity.[22]

The outflow speed v_{out} is measured as the average of the maximum outflow speed in either outflow direction. By a similar argument as for E, Eq. (1) gives

$$v_{\text{out}}\left[\frac{\rho_1}{\rho_1(\text{Sym})}\right]^{1/2} \sim v_{\text{out}}(\text{Sym})\left(\frac{2}{1+\rho_2/\rho_1}\right)^{1/2}, \tag{25}$$

where $v_{\text{out}}(\text{Sym})$ is the value from the symmetric run. As such, a plot of $v_{\text{out}}\rho_1^{1/2}$ against ρ_2/ρ_1 should have the data collapse to a single curve. The data are plotted in Fig. 5(b) with the prediction plotted as the dashed line. Again, there is good agreement with the theory.

The half-thickness δ of the dissipation region is measured as the half-width at half-maximum of the out-of-plane current density J_z in a cut across the *X*-line. From Eq. (11) applied to the case with symmetric fields,

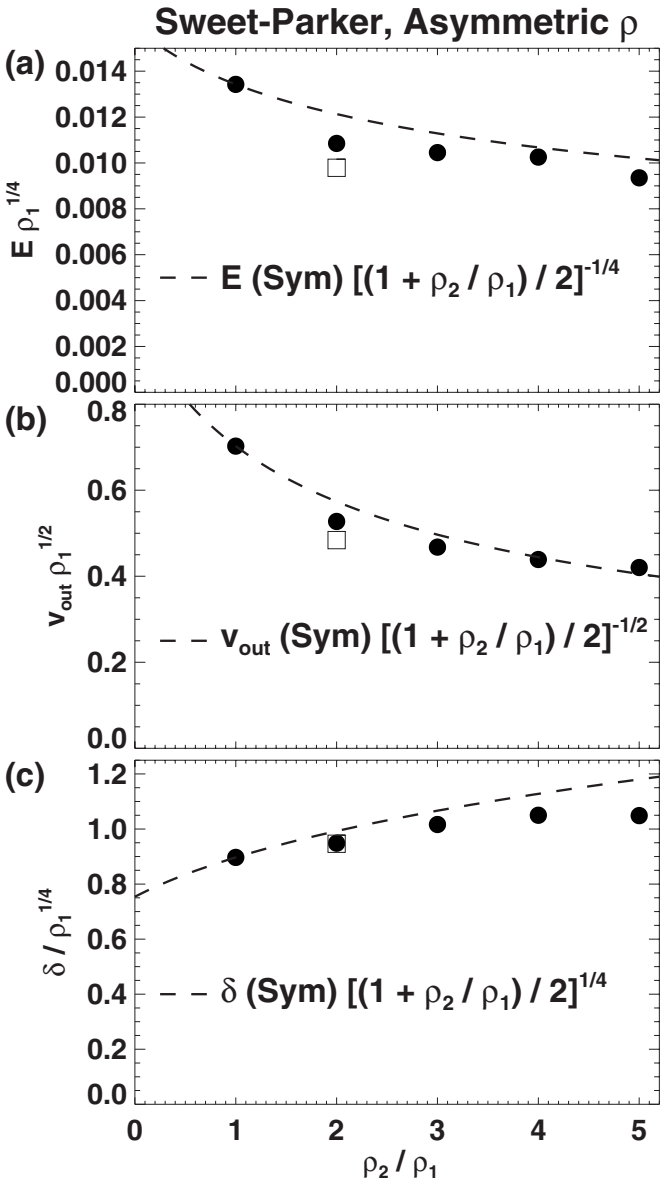

FIG. 5. Scaling results for asymmetric density Sweet–Parker simulations. Plotted as a function of density ratio ρ_2/ρ_1 are the (a) reconnection rate E (normalized to $\rho_1^{-1/4}$), (b) outflow velocity v_{out} (normalized to $\rho_1^{1/2}$), and (c) half-thickness δ of the dissipation region (normalized to $\rho_1^{1/4}$). The solid dots have $\rho_1=\rho_0$; the open box has $\rho_2=2\rho_0$. The dashed lines are the predictions from the theory.

$$\delta\left[\frac{\rho_1(\mathrm{Sym})}{\rho_1}\right]^{1/4} \sim \delta(\mathrm{Sym})\left(\frac{2}{1+\rho_2/\rho_1}\right)^{1/4}, \tag{26}$$

where δ(Sym) is the value from the symmetric simulation, so plotting $\delta/\rho_1^{1/4}$ against ρ_2/ρ_1, should have the data collapse to a single curve. The data are plotted in Fig. 5(c), with the prediction plotted as the dashed line. The agreement is good, but not great.

We turn to the interior structure of the dissipation region. Plotted in Fig. 6 are δ_{S1} and δ_{S2}, measured directly by finding the stagnation point and evaluating the distance to the upstream edges of the sheet. The plot clearly shows the equality of the two distances, which directly contradicts the prediction in Eq. (9) [but coincidentally agrees with Eq. (23) evaluated for symmetric fields]. The distances δ_{X1} and δ_{X2} (measured directly as the distance from the upstream edges to the X-line, not plotted) are essentially equivalent to δ_{S1} and δ_{S2}, respectively.

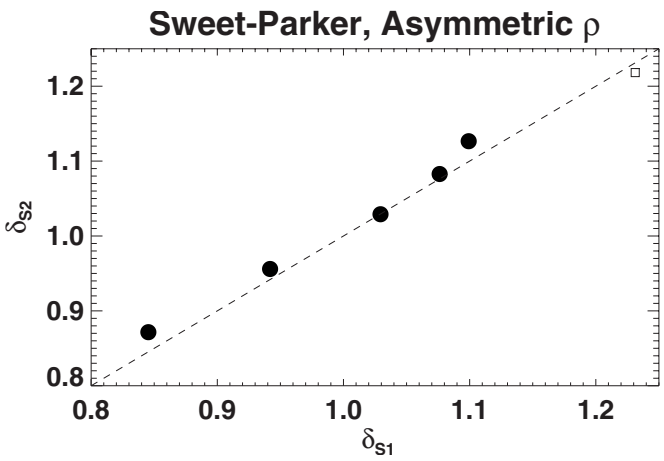

FIG. 6. Distance from the stagnation point to the edge of the dissipation region above (δ_{S1}) and below (δ_{S2}) for asymmetric density Sweet–Parker simulations. Solid dots have $\rho_1=\rho_0$; the open box has $\rho_1=2\rho_0$. The dashed line denotes the two distances being equal. This result disagrees with Eq. (9). Data for δ_{X1} and δ_{X2} are almost identical (not shown).

In summary, the clear indication from both the Sweet–Parker and Hall reconnection simulations is that the location of the X-line is well predicted by the theory, but the location of the stagnation point is not when the densities are asymmetric, corroborating Ref. 23. An explanation for the discrepancy is presented in Sec. IV.

IV. DISCUSSION

The present results, in addition to previous results,[23] reveal that there is an inconsistency between the theoretical prediction in Eq. (9) and the simulation results, at least when the density is asymmetric. [When the density is symmetric, the agreement is good, as can be seen from the (blue) squares in Fig. 4 and MHD results in Ref. 19.]

We now argue that the discrepancy is caused by a deficiency in the fluid description of a plasma enlisted in the present and previous simulations. When flux tubes on either side of the dissipation region reconnect, the plasmas are free to mix along the newly reconnected magnetic field line. The expression giving the density of the plasma in the outflow, Eq. (9), is predicted on the assumption that the plasmas mix completely before leaving the dissipation region, as discussed after Eq. (3).

Consider, however, the case with asymmetric density but symmetric magnetic fields. Since the magnetic field is symmetric, the total gas pressure $P \propto \rho T$ must also be symmetric, where T is the temperature. As such, the plasma in the newly reconnected flux tube is at equal gas pressure above and below the neutral line, as illustrated in Fig. 7. Of course, in a real plasma (or in a kinetic description of a plasma), the high T and low ρ plasma mixes with the low T and high ρ plasma, as observed in hybrid simulations of asymmetric reconnection.[33] However, in a fluid description, the two plas-

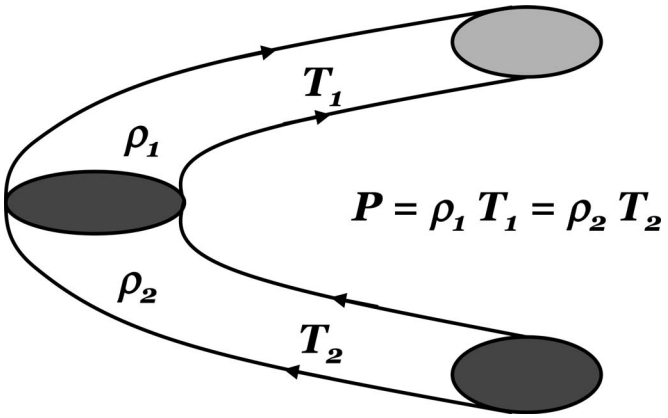

FIG. 7. Schematic showing a newly reconnected flux tube. While pressure is balanced in the fluid sense, mixing between the plasmas will occur due to kinetic effects.

mas are in pressure balance, so no mixing occurs (unless heat conduction along the field lines is included in the fluid description).

The effects of nonmixing are manifested in the outflow region of the dissipation region during Hall reconnection with asymmetric density. As the plasma flows in the outflow direction at Alfvénic speeds, it passes through a region with a strong density gradient (because mixing has not smoothed it). This drives an instability, as seen in Fig. 8. The roll patterns persist as the ejected plasma becomes trapped in the magnetic island. However, it is transient in the region immediately downstream of the dissipation region, becoming smooth at late times.

The instability is also present in asymmetric Sweet–Parker simulations, noticeably in the asymmetric density runs in the island just past the outflow edge of the dissipation region (not shown). For simulations with asymmetric field but initially symmetric density (for both Sweet–Parker and Hall reconnections), a small density gradient is self-consistently generated and goes unstable to the same instability. A similar instability has been observed in Ref. 50. These instabilities should be the topic of future study, as they may be important for generating turbulence and mixing plasma in outflow jets and magnetic islands. However, they may also be unphysical, arising from the lack of mixing in fluid codes. Indeed, the instability has not been observed in PIC simulations of asymmetric reconnection,[26–29] although this may be an artifact of the use of small system sizes.

To show how a lack of plasma mixing changes the dissipation region substructure, consider how the theory changes if plasma mixing is not permitted. One can show that the predictions for v_{out} and E in Eqs. (1) and (2) are unchanged with a different distribution of outflow density. However, Eqs. (6) and (7) become

$$L(\rho_1 v_1) \sim \delta_{S1}(\rho_1 v_{\text{out}}), \tag{27}$$

$$L(\rho_2 v_2) \sim \delta_{S2}(\rho_2 v_{\text{out}}), \tag{28}$$

i.e., the outflow density is the density on the appropriate side because of the lack of mixing. The densities cancel, so their ratio immediately gives

$$\frac{\delta_{S2}}{\delta_{S1}} \sim \frac{B_1}{B_2}. \tag{29}$$

This result is precisely the relationship given in Eq. (23) which agrees with the asymmetric density simulations in Hall [see Fig. 4(e)] and Sweet–Parker (see Fig. 6) reconnection. This result is also qualitatively consistent with numerical results from Ref. 23 in that the location of the stagnation point and X-line are independent of the density ratio (see their Fig. 8), although it does not quantitatively agree with their results. This could be due to their use of a localized η, but further study is warranted.

It should be emphasized that while the nonmixing of plasmas in fluid simulations potentially explains why the stagnation point is at the center of the dissipation region in

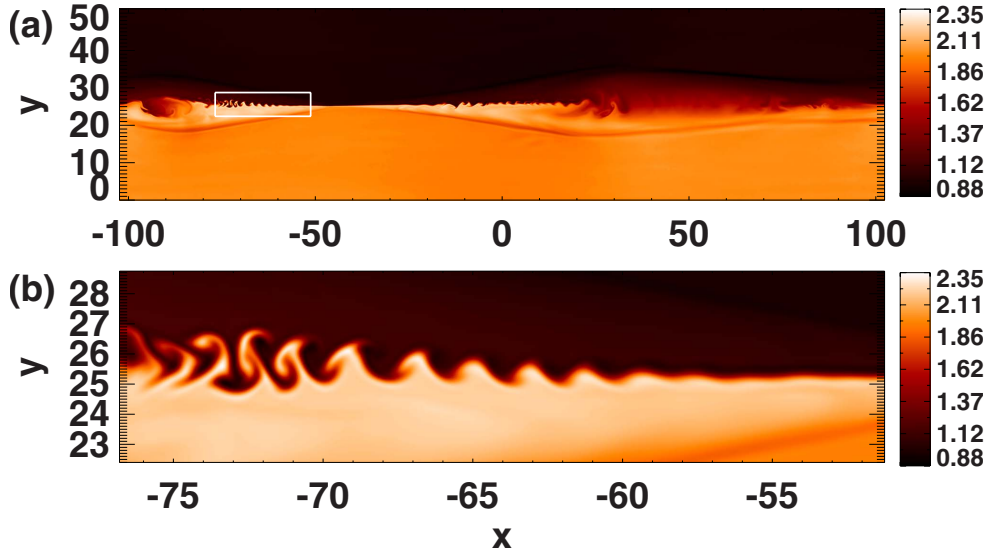

FIG. 8. (Color online) Grayscale of the plasma density ρ during two-fluid simulations with a density asymmetry of 2 (run *HN*1). (a) The upper half of the computational domain; (b) a zoom in of the outflow region denoted by the white box in (a).

asymmetric density simulations, it introduces other problems. In a theory without mixing, Eqs. (4) and (5) are modified, as well. As a result, the location of the X-line given in Eq. (8) is not a result of the nonmixing theory, yet this expression agrees with the simulations. As such, neither the full mixing theory of Ref. 19 nor the nonmixing theory of this section can explain the results of the fluid simulations.

What remains to be seen is whether the disagreement between the theory and the fluid simulation results is a failure of the theory or a failure of the fluid model used in the simulations. We suspect that the failure lies in the fluid description that omits parallel heat conduction and suggest that more sophisticated kinetic simulations will likely be necessary to obtain definitive answers. As such, the extent to which mass continuity, gyroradius effects, and plasma mixing conspire to control the internal structure of the dissipation region remains an open question.

V. SUMMARY AND CONCLUSIONS

This paper reports results of a study of the scaling of the structure of the dissipation region during asymmetric magnetic reconnection. The theory and simulations are restricted to two dimensions with antiparallel magnetic fields. The results of the study, put in the context of previous studies, are as follows.

- Predictions for the scaling of the outflow speed v_{out} [Eq. (1)] and reconnection rate E [Eq. (2)] presented in Ref. 19 are in agreement with MHD simulations of with asymmetric density (present paper) and asymmetric field[19] and with two-fluid simulations with either or both density and field asymmetric.[25] The prediction for E also agrees with MHD[22–24] and PIC (Ref. 26) simulations.
- The prediction for the thickness δ of the dissipation region [Eq. (11)] during asymmetric Sweet–Parker reconnection is borne out in simulations of asymmetric density (present paper) and field.[19]
- We present a physical model for the thickness of the dissipation region during Hall reconnection [Eq. (17)]. Two-fluid simulation results are consistent with the theory. In summary, the predictions for E, v_{out}, and δ are rather successful.
- The predictions for the location of the X-line [Eq. (8)] and stagnation point [Eq. (9)] are well borne out by Sweet–Parker[19] and Hall (present paper) simulations for asymmetric fields with symmetric density. However, simulations with asymmetric density disagree with the theory (present paper). They always show that the X-line is located at the center of the dissipation region. This disagreement corroborates a result of Ref. 23.
- We propose that the cause of the discrepancy is the failure of fluid codes to capture the physics of plasma mixing along a newly reconnected field line. We claim that fluid simulations (MHD and two-fluid) without parallel heat conduction are fundamentally incapable of providing reliable information about the substructure of the dissipation region in asymmetric reconnection when the density is asymmetric. More advanced simulation models, such as PIC or hybrid, are necessary to determine the substructure of the dissipation region.
- A fast flow across a strong density gradient in the outflow region produces an instability in the outflow region. Further studies are required to determine if this instability is an artifact of the lack of mixing in fluid codes or is genuinely physical.

The results have potential applications to reconnection events at the dayside magnetopause. A recent study[30] observed a (full width) magnetopause thickness of $\sim$150 km which was reported as two to three times the ion inertial length based on the average density of $\sim$62.5 km. Equation (17) predicts a full thickness $2\delta \sim 133$ km (using $n_1 \sim 25$ cm^{-3}, $n_2 \sim 1.5$cm^{-3}, $B_1 \sim 10$ nT, and $B_2 \sim 50$ nT). The estimate presented here represents the data slightly more faithfully than the length based on the average density. Of course, a more thorough scaling study of many events at the magnetopause will be necessary to make any conclusive statements, but the agreement is encouraging.

Limitations of the present MHD simulations include using uniform resistivity instead of Spitzer resistivity and not including Joule heating. For the two-fluid simulations, the implementation ignores density gradients on electron scales. Also, the choice of grid scale precludes the use of asymmetries larger than 3.[25] Checking scaling for higher asymmetries requires more computational resources. Finally, as emphasized in Sec. III, both fluid models lack parallel heat conduction, which is important within the dissipation region.

Future work should use kinetic simulations to study the scaling of the structure of the dissipation region and E and v_{out} predicted here and in Ref. 19. Such simulations may be complicated as there is no known kinetic equilibrium for asymmetric systems[26] and the temperature asymmetries lead to a large degree of noise. An observational study of multiple crossings to ascertain the scaling would also be very useful. The nature of the instability in the outflow region should be tested with PIC codes, as the previous simulations[26–29] used system sizes not larger than $25d_{i0}$, rendering it unlikely that the simulations would have seen this effect if it is present.

Additional studies should involve relaxing the simplifying assumptions of the model, such as the two dimensionality and that the magnetic fields are antiparallel. It has been established that a density gradient across the dissipation region introduces diamagnetic drifts which reduce the reconnection rate.[21,51] Also, disparate theories predicting the plane that reconnection occurs between fields of arbitrary direction have been offered[34,52] but it has not been resolved numerically.

ACKNOWLEDGMENTS

This work was supported by NASA Grant Nos. NNX08AO83G and NNX08AM37G, and NSF Grant No. ATM-0645271. Computations were carried out at the National Energy Research Scientific Computing Center.

[1] J. W. Dungey, Philos. Mag. **44**, 725 (1953).
[2] P. A. Sweet, in *Electromagnetic Phenomena in Cosmical Physics*, edited by B. Lehnert (Cambridge University Press, New York, 1958), p. 1237.

[3]E. N. Parker, J. Geophys. Res. **62**, 509, DOI: 10.1029/JZ062i004p00509 (1957).
[4]H. E. Petschek, in *AAS/NASA Symposium on the Physics of Solar Flares*, edited by W. N. Ness (NASA, Washington, DC, 1964), p. 425.
[5]R. H. Levy, H. E. Petschek, and G. L. Siscoe, AIAA J. **2**, 2065 (1964).
[6]T. D. Phan and G. Paschmann, J. Geophys. Res. **101**, 7801, DOI: 10.1029/95JA03752 (1996).
[7]H. C. Ku and D. G. Sibeck, J. Geophys. Res. **102**, 2243, DOI: 10.1029/96JA03162 (1997).
[8]F. Mozer, S. D. Bale, and T. D. Phan, Phys. Rev. Lett. **89**, 015002 (2002).
[9]F. Mozer and A. Retinó, J. Geophys. Res. **112**, A10206, DOI: 10.1029/2007JA012406 (2007).
[10]J. E. Borovsky and J. T. Steinberg, J. Geophys. Res. **111**, A07S10, DOI: 10.1029/2005JA011397 (2006).
[11]J. E. Borovsky and M. H. Denton, Geophys. Res. Lett. **33**, L20101, DOI: 10.1029/2006GL026519 (2006).
[12]J. Sanny, C. Beck, and D. G. Sibeck, J. Geophys. Res. **103**, 4683, DOI: 10.1029/97JA03246 (1998).
[13]M. Øieroset, T. D. Phan, and M. Fujimoto, Geophys. Res. Lett. **31**, L12801, DOI: 10.1029/2004GL019958 (2004).
[14]J. T. Gosling, S. Eriksson, R. M. Skoug, D. J. McComas, and R. J. Forsyth, Astrophys. J. **644**, 613 (2006).
[15]V. V. Mirnov, C. C. Hegna, S. C. Prager, C. R. Sovinec, and H. Tian, IAEA FEC Conference, China, 2006 (unpublished), Paper No. TH–P3–18.
[16]N. A. Murphy and C. R. Sovinec, Phys. Plasmas **15**, 042313 (2008).
[17]M. Ugai, Phys. Plasmas **7**, 867 (2000).
[18]S. Servidio, W. H. Matthaeus, M. A. Shay, P. A. Cassak, and P. Dmitruk, Phys. Rev. Lett. **102**, 115003 (2009).
[19]P. A. Cassak and M. A. Shay, Phys. Plasmas **14**, 102114 (2007).
[20]H. Karimabadi, D. Krauss-Varban, N. Omidi, and H. X. Vu, J. Geophys. Res. **104**, 12313, DOI: 10.1029/1999JA900089 (1999).
[21]M. Swisdak, J. F. Drake, M. A. Shay, and B. N. Rogers, J. Geophys. Res. **108**, 1218, DOI: 10.1029/2002JA009726 (2003).
[22]J. E. Borovsky and M. Hesse, Phys. Plasmas **14**, 102309 (2007).
[23]J. Birn, J. E. Borovsky, and M. Hesse, Phys. Plasmas **15**, 032101 (2008).
[24]J. E. Borovsky, M. Hesse, J. Birn, and M. M. Kuznetsova, J. Geophys. Res. **113**, A07210, DOI: 10.1029/2007JA012645 (2008).
[25]P. A. Cassak and M. A. Shay, Geophys. Res. Lett. **35**, L19102, DOI: 10.1029/2008GL035268 (2008).
[26]P. L. Pritchett, J. Geophys. Res. **113**, A06210, DOI: 10.1029/2007JA012930 (2008).
[27]K. G. Tanaka, A. Retino, Y. Asano, M. Fujimoto, I. Shinohara, A. Vaivads, Y. Khotyaintsev, M. Andre, M. B. Bavassano-Cattaneo, and C. J. Owen, Ann. Geophys. **26**, 2471 (2008).
[28]J. Huang, Z. W. Ma, and D. Li, Geophys. Res. Lett. **35**, L10105, DOI: 10.1029/2008GL033751 (2008).
[29]J. Huang and Z. W. Ma, Chin. J. Geophys. **51**, 960 (2008).
[30]F. S. Mozer, V. Angelopoulos, J. Bonnell, K. H. Glassmeier, and J. P. McFadden, Geophys. Res. Lett. **35**, L17S04, DOI: 10.1029/2007GL033033 (2008).
[31]F. S. Mozer, P. Pritchett, J. Bonnell, D. Sundqvist, and M. Chang, J. Geophys. Res. **113**, A00C03, DOI: 10.1029/2008JA013535 (2008).
[32]J. E. Borovsky, J. Geophys. Res. **113**, A08228, DOI: 10.1029/2007JA012646 (2008).
[33]M. Nakamura and M. Scholer, J. Geophys. Res. **105**, 23179, DOI: 10.1029/2000JA900101 (2000).
[34]M. Swisdak and J. F. Drake, Geophys. Res. Lett. **34**, L11106, DOI: 10.1029/2007GL029815 (2007).
[35]V. M. Vasyliunas, Rev. Geophys. **13**, 303, DOI: 10.1029/RG013i001p00303 (1975).
[36]B. U. Ö. Sonnerup, in *Solar System Plasma Physics*, edited by L. J. Lanzerotti, C. F. Kennel, and E. N. Parker (North-Holland, Amsterdam, 1979), Vol. 3, p. 46.
[37]M. A. Shay, J. F. Drake, R. E. Denton, and D. Biskamp, J. Geophys. Res. **103**, 9165, DOI: 10.1029/97JA03528 (1998).
[38]Y. Ren, M. Yamada, S. Gerhardt, H. Ji, R. Kulsrud, and A. Kuritsyn, Phys. Rev. Lett. **95**, 055003 (2005).
[39]C. D. Cothran, M. Landreman, M. R. Brown, and W. H. Matthaeus, Geophys. Res. Lett. **32**, L03105, DOI: 10.1029/2004GL021245 (2005).
[40]A. G. Frank, S. Y. Bogdanov, G. V. Dreiden, V. S. Markov, and G. V. Ostrovskaya, Phys. Lett. A **348**, 318 (2006).
[41]M. A. Shay, J. F. Drake, M. Swisdak, and B. N. Rogers, Phys. Plasmas **11**, 2199 (2004).
[42]A. Retinó, A. Vaivads, M. André, F. Sahraoui, Y. Khotyaintsev, J. S. Pickett, M. B. B. Cattaneo, M. F. Marcucci, M. Morooka, C. J. Owen, S. C. Buchert, and N. Cornilleau-Wehrlin, Geophys. Res. Lett. **33**, L06101, DOI: 10.1029/2005GL024650 (2006).
[43]G. L. Siscoe, G. M. Erickson, B. U. O. Sonnerup, N. C. Maynard, J. A. Schoendorf, K. D. Siebert, D. R. Weimer, W. W. White, and G. R. Wilson, Geophys. Res. Lett. **29**, 1626, DOI: 10.1029/2001GL013536 (2002).
[44]M. Hoshino and A. Nishida, J. Geophys. Res. **88**, 6926, DOI: 10.1029/JA088iA09p06926 (1983).
[45]M. Scholer, J. Geophys. Res. **94**, 8805, DOI: 10.1029/JA094iA07p08805 (1989).
[46]J. C. Dorelli, M. Hesse, M. M. Kuznetsova, L. Rastaetter, and J. Raeder, J. Geophys. Res. **109**, A12216, DOI: 10.1029/2004JA010458 (2004).
[47]A. L. La Belle-Hamer, A. Otto, and L. C. Lee, J. Geophys. Res. **100**, 11875, DOI: 10.1029/95JA00969 (1995).
[48]E. R. Priest, V. S. Titov, R. E. Grundy, and A. W. Hood, Proc. R. Soc. London, Ser. A **456**, 1821 (2000).
[49]R. P. Rijnbeek, V. S. Semenov, A. A. Shmalts, H. K. Biernat, M. F. Heyn, and B. P. Besser, Planet. Space Sci. **39**, 1377 (1991).
[50]D. Grasso, D. Borgogno, and F. Pegoraro, Phys. Plasmas **14**, 055703 (2007).
[51]K. Germaschewski, A. Bhattacharjee, C. S. Ng, X. Wang, and L. Chacon, Bull. Am. Phys. Soc. **51**, 312 (2006).
[52]B. U. Ö. Sonnerup, J. Geophys. Res. **79**, 1546, DOI: 10.1029/JA079i010p01546 (1974).